Journal of Power Sources 268 (2014) 194–203

Contents lists available at ScienceDirect

Journal of Power Sources

journal homepage: www.elsevier.com/locate/jpowsour

Experimental investigation of two-phase flow pressure drop transients in polymer electrolyte membrane fuel cell reactant channels and their impact on the cell performance

Rupak Banerjee, Satish G. Kandlikar*

Mechanical Engineering and Microsystems Engineering, Rochester Institute of Technology, Rochester, NY 14623, USA

HIGHLIGHTS

- Established relationship between two-phase transients and channel pressure drop.
- Effect of two-phase transients on voltage response of the cell is investigated.
- Effects of current density and temperature changes have been decoupled.
- Overshoot behavior observed in two-phase pressure drop following a transient event.

ARTICLE INFO

Article history:
Received 3 December 2013
Received in revised form
15 May 2014
Accepted 22 May 2014
Available online 12 June 2014

Keywords:
PEM fuel cell
Transient behavior
Pressure drop
Voltage response
Load
Temperature

ABSTRACT

Fuel cells experience transients, which constitute a significant part of the drive cycle. Fuel cell response during these transients depends on the rates of reaction kinetics as well as mass transport delays. In the current work, an in situ setup is used to investigate the effect of changing load and temperature conditions on the two-phase flow in the fuel cell. Pressure drop and voltage response from the cell are used to characterize the two-phase flow and performance of the cell. The effect of changing load is simulated by changing the current by 20 A cm^{-2} (0.4 A cm^{-2}) over a time period of 300 s, while the effect of changing cell temperature is studied by increasing/decreasing the cell temperature by 40 °C over 900 s. The results show that several minutes are required after a transient event for the two-phase flow to return to a new steady state condition. Transient effects are more prominent at the lower temperature of 40 °C, at which condition there is more liquid water present in the channels. Overshoot behavior, commonly seen in current and voltage response from fuel cells, has been observed for two-phase pressure drop during transient load changes.

1. Introduction

Proton Exchange Membrane fuel cells (PEMFCs) are being considered as a viable replacement for the internal combustion (IC) engines for automotive transportation. The possibility of rapid refueling and extended range of PEMFC vehicles make them attractive over Battery Electric Vehicles (BEVs). The low operating temperature, rapid start up and high power density make them a desirable option for portable power generation units as well. Automotive transportation powertrains are expected to respond to rapid changes in speed/acceleration and therefore are designed for a rapid power output response [1,2]. The current work investigates the water management of fuel cells during transient operating conditions with changing load and temperature conditions.

Currently, PEMFCs are used in conjunction with a conventional battery, which supplements the power during high demand and stores the excess and regenerated power during low demand. However, relying on batteries entirely results in excess vehicular weight and lower system efficiency. The requirement for large energy storage devices on board can be reduced significantly by improving the response time from the PEMFC, and making the powertrain "load-following" [3,4].

Significant research efforts have been directed towards understanding the steady state performance of PEMFCs in the past two decades, while only a limited number of studies are devoted to the transient response. A brief literature review is presented here with the focus on the transient behavior of PEMFCs. Amphlett et al. [5]

* Corresponding author. Tel.: +1 585 475 6728; fax: +1 585 475 7710.
E-mail addresses: rxb5214@rit.edu (R. Banerjee), sgkeme@rit.edu (S.G. Kandlikar).

http://dx.doi.org/10.1016/j.jpowsour.2014.05.123
0378-7753/

developed the first transient model, highlighting the effect of varying temperature on the cell performance. They introduced a heat accumulation term to generate the transient information during start-up, shut-down or step changes in current. Pakrushpan et al. [6] developed a model for the entire automotive fuel cell system based on the transient characteristics of the flow dynamics. Although the model components were verified, the complete model was not validated in their work due to non-availability of transient experimental data. Song et al. [7] and Yan et al. [8] investigated the effect of liquid water transport on the cathode side and its effect on the transient behavior. Both groups used analytical models for their investigation. They concluded that less liquid water in the system results in longer transient time periods. High current density, increased water saturation of the Gas Diffusion Layer (GDL), and more liquid water in the channels all reduced the time to reach a new steady state condition. A lower inlet relative humidity was seen to increase the transient time duration, while a thinner membrane had an opposite effect.

Several authors have used numerical techniques to probe the transient behavior of PEMFC systems. Wang and Wang [9] investigated the drying phenomenon of the GDL and the membrane under the application of dry gases, and observed that the cell voltage dropped by 100 mV over 20 s under the influence of dry gases. The cathode side showed a more prominent transient behavior, highlighting the need for further investigation into cathode transients. Meng [10] demonstrated the impact of GDL saturation on the overshoot or undershoot of current during transients. The overshoot tendency was more prominent under two-phase condition compared to single-phase condition. This was attributed to change in liquid water saturation in the GDL which changes the mass transport resistance. The time required for the saturation to reach a new steady state value results in the overshoot.

Corbo et al. [3,11] investigated the behavior of PEMFCs under transient conditions by mimicking the European R40 and R47 drive cycles and obtained a system efficiency of 40%. Hamelin et al. [12] matched their data with the model of Amphlett et al. [5], confirming that the water content of the membrane took several minutes to reach equilibrium and resulted in an increased time duration of transient response from the PEMFC. Tang et al. [13] focused their work on the electrochemical transients. The electrical load on the cell was changed and the overshoot and undershoot of voltage during the transient time duration were observed. The findings were attributed to the charging and discharging of the electrical double layer.

Yan et al. [8] highlighted the major problems encountered during transients. Rapid changes in load result in voltage undershoot which leads to reversal in polarity of the PEM voltage. Repeated reversals may result in an increase in catalyst degradation [14]. Yan et al. [8] also showed that rapid current density changes do not allow a full recovery of the flow conditions in the flow field. High stoic ratios and high operating pressures were beneficial in reducing the transient time. Kim et al. [15] also showed that high stoic ratios reduce the well documented overshoot/undershoot behavior of voltage during transients. Chen and Zhou [16] conducted experiments and noted the transient conditions to be most prominent at the start up. Kim et al. [17] and Francesco and Arato [18] used PEMFC stacks to investigate the transient response, and reported a gradual increase in temperature with an increase in power. Kim et al. [17] showed that an increasing load protocol had a much shorter transient compared to a decreasing load protocol. Rabbani and Rokni [19] developed a control oriented model which showed that although the auxiliary systems consume only 10% of the generated power at steady state, they consume up to 15% of the power during transient operation. Thus, transient operation increased the auxiliary power consumption, lower system efficiency and increase catalyst degradation.

Transient operation of fuel cells leads to several mechanisms of degradation. The membrane (PEM) suffers more from cyclic loading compared to constant operation, as demonstrated by Liu and Case [20]. At the end of 1000 h of operation, the MEA subjected to cyclic loading resulted in increased hydrogen cross-over whereas the MEA operated at constant current had a larger mass transport resistance but performed better than the earlier case. Lin et al. [21] also found physical degradation (cracks and pin-hole formation) of the membrane resulting from operating the cell under dynamic drive cycles. Detailed reviews of the mechanisms for degradation of the catalyst layers are provided by Wu et al. [22] and Schmittinger and Vahidi [23]. With dynamic cycles, occurrence of cell flooding, reactant starvation and local hotspots are increased. Reactant starvation is a primary cause for carbon corrosion and leads to loss in durability of the catalyst [22]. Reactant starvation is likely to introduce cell reversal which promotes carbon corrosion.

Chang and Chu [24] showed that although the initial transients are dominated by the electrochemical process, which reaches steady state within one second. Beyond this one second time period, the current density begins to fluctuate again and is attributed to the two-phase effects. Wu et al. [25] numerically investigated the impact of liquid water on the reactant concentration profiles at the catalyst layer. At start up, no water blockage is assumed with the concentration decreasing with an increase in water generation rate. However, they established that the concentration profiles reach steady state within the first two seconds under all conditions. Experimental validation of these findings is warranted. Chen et al. [26] investigated the time for the membrane water content to reach a steady state condition after a transient event. The time required to reach a steady state was observed for different current density changes. They found that the time required to reach a new steady state decreases at the higher current densities. They attributed it to the higher water generation rates which help in maintaining a high membrane hydration, and reduce the duration after transient events.

Pressure drop has been shown to be a good diagnostic tool for identifying the presence of liquid water in the PEMFC [27–29]. Pressure drop has been used to characterize the two-phase flow patterns in both in situ and ex situ studies [30–35]. The development of water features and their motion can also be detected using pressure drop signatures [31,33,34]. Cheah et al. [33] used pressure drop signatures to characterize the growth of a droplet into a slug in a millimeter scale channel. They used force balance analysis to show that more energy is required to remove water features at higher gas flow rates. In a complimentary work [35], the authors discussed the comparison of slug formation in rectangular, square and semi-cylindrical channels. A lower pressure drop was observed for semi-cylindrical channels. Hellstern et al. [34] investigated the role of the GDL in slug formation in a single channel setup, demonstrating a more gradual build-up of the slug and a lower pressure drop in removing the slug, in the presence of a GDL. However the slug remained pinned for a longer duration. Rath and Kandlikar [36] identified the channel corner with the GDL to be an important parameter in analyzing the behavior of droplet growth to form slugs in mini and micro channels. Gopalan and Kandlikar [37,38] investigated the impact of corner filling criterion on the droplet growth with gas flow and suggested the use trapezoidal channels with 50° corner angle for use in automotive fuel cells for improving the water removal process. They also modeled this interaction between the wall and the droplet using an energy balance method [39]. Their work was key to establishing the area of GDL blocked to reactant diffusion and the channel cross sectional area blocked for gas flow.

The water features commonly observed in PEMFC reactant channels are slug flow, film flow and mist flow. Slug flow tends to

block the entire channel, while film flow only creates a partial constriction in the channel. In the case of mist flow, water particles are carried in the gas stream as a homogeneous mixture. Mist flow does not block any interfacial area on the GDL available for reactant diffusion. A detailed discussion on the flow patterns observed in the reactant channels of PEMFCs is provided by Grimm et al. [40].

Anderson et al. [41] reviewed two-phase flow in the PEMFC reactant channels. They compared in situ studies, ex situ experiments as well as numerical modeling approaches in dealing with two-phase flow in the reactant channels. In all cases, the lower superficial gas velocities resulted in slug flow, while the highest gas flow rates showed mist flow. The intermediate region was dominated by film flow.

Tuber et al. [42] and Sergi and Kandlikar [43] both used in situ visualization setup to investigate the two-phase flow in the reactant channels. Tuber et el. presented qualitative information, while the latter went further and used image processing techniques in quantifying the liquid water present in the reactant channels at different operating conditions. Banerjee and Kandlikar [44] conducted a parametric study in an ex situ environment. All three showed that increasing the gas velocity reduces the water residence time in the channels. This resulted in a lower average liquid water coverage. Banerjee and Kandlikar [44] also showed that most of the operating range of PEMFCs is dominated by film flow.

At ambient temperatures, there is a significant contribution of slug flow, and all three of the flow patterns are observed [31,32]. Changing the channel cross section and surface energy of the channels modifies the flow pattern maps that have been obtained. Adroher and Wang [45] investigated the two-phase flow pattern maps in a single channel ex situ setup and established that they matched up with the multi-channel results presented by Lu et al. [31]. However, as temperature is increased above from ambient conditions, the tendency for slug flow is significantly decreased, and the dominant flow pattern being film flow for most of the conditions [44].

Steinbrenner et al. [46] focused on the impact of the flow field and the GDL on the two-phase flow patterns dominant in the reactant channels. Their work showed that the presence of sharp corners in the flow field (such as in serpentine flow fields) can result in change in flow regimes due to the influence of the corners. The impact of flow orientation (with regard to gravity) was investigated by Zhang et al. [47]. They showed that the tendency of slug formation was more in the case of flow opposing the gravitation pull. Lu et al. [32] showed that horizontally oriented channels were more susceptible to slug flow compared to vertically oriented channels with the flow direction in favor of gravity.

Water management in PEMFCs is not isolated from the thermal management. Kandlikar and Lu [48] highlighted the close relationship between water and thermal management, and the impact of temperature non-uniformity on the change in the mode of water transport throughout the PEMFC layers. Tiss et al. [49] introduced a non-isothermal model for the prediction of cell voltage. Yan et al. [50] used numerical modeling to highlight the temperature dependence of PEMFC performance and its impact on water management. They concluded that increasing temperature and current density introduces dehydration on the anode side due to increased electro-osmotic drag. The temperature distribution also changed sharply at high current densities resulting in damage to the membrane and uneven current and water distributions.

Kim et al. [17] used a 1.2 kW Nexa PEMFC stack from Ballard Power Systems and developed a model based on their experimental results. By applying cyclic current step functions fluctuating between 5 A and 25 A, the output voltage and temperature was observed. Both the output voltage and the stack temperature followed the changes in current load. The temperature profile follows a saw–tooth profile with temperature increasing with an increase in load and decreasing when the load is decreased. The temperature takes several minutes to reach a new steady state condition; this time duration is significantly longer compared to the electrochemical transients as discussed earlier. Additionally, the results show that due to the time needed for the temperature to reach a new steady state value, the voltage too requires significantly longer duration to reach steady state. Banerjee and Kandlikar [44] explored the impact of temperature on the liquid water present in the reactant channels and showed that an increase in temperature reduces the liquid water coverage on the GDL. Therefore the area available for reactant diffusion increases with increase in temperature since there is less water present in the reactant channels.

From the above review of existing literature, it can be summarized that transient operation consumes more power than steady state operation. Temperature increases slowly with increased power generation. However, the increase in temperature is a relatively slow process and therefore introduces long periods of transient behavior. It has also been established that the two-phase behavior within PEMFCs depends on the temperature of the cell, and the quantity of liquid water within the GDL and the channels plays a key role. However, the relationship between the voltage response and the two-phase flow within the PEMFC has not been explored under transient conditions.

The current work investigates the transient behavior of two-phase flow in the reactant channels using pressure drop as the characteristic parameter. The voltage response from the cell is used to characterize the performance. The effect of rapidly increasing and decreasing temperature on the two-phase pressure drop and the cell voltage is explored. Pressure drop responses from load changes are studied at three different temperatures. Two-phase pressure drop is compared for transient and steady state load conditions. The focus of the investigation is to obtain a better understanding of the two-phase flow behavior during transient operation of the PEMFC. Preliminary results from this investigation were presented in an earlier work [51].

2. Experimental setup

An in situ test setup was used in the current investigation. The discussion of the experimental setup is divided into three sections. The first section covers the fuel cell and its components. The second section delves into the testing system, including the fuel cell test stand and the auxiliary systems. The third section discusses the accuracy of the measurement systems and the uncertainty of the results.

2.1. Test cell

A fuel cell has been manufactured and assembled in house at RIT. The cell had an active area of 50 cm^2 with a Gore membrane (18 μm thick) and MRC 105 GDL (230 μm thick) on both sides. The GDL had 5 wt. % PTFE loading and was coated with an MPL on one side. The MPL coating was applied by General Motors (GM) using a proprietary process. The current collector plates house the gas channels and were fabricated in copper. They were then coated with gold to minimize contact resistance. The flow field consisted of straight channels with 5° of switchback as described by Owejan et al. [52]. The reactant delivery channels were 700 μm wide and 400 μm deep. The inlet and outlet manifolds were equipped with pressure taps to measure the overall pressure drop along the length of the channels. The compression plates also house serpentine coolant channels, and are divided into four sections along the length of the channels to provide a uniform cell temperature. Water is used as the coolant in the compression plates.

2.2. Test equipment

Fig. 1 shows a schematic of the fuel cell test setup used in the current system. A Greenlight Technology's G40 test stand was used to control the test conditions and record the data. The test stand provided the desired gas flow rates at the specified temperature and relative humidity. For this investigation, the test stand was operated in a constant stoic mode in which a constant stoichiometry was maintained for a given load condition. The test conditions are discussed in further detail in Section 4. Automated testing is made possible through HyAl Fuel Cell Automated Testing System (FCATS), which is used for ramped load changes during the investigation. Load, cell voltage, dew point temperature and gas temperature were measured at the test stand.

Gas lines between the test stand and the fuel cell were equipped with auxiliary heating to maintain a constant gas temperature and avoid any condensation in the supply lines. The fuel cell temperature was maintained by circulating coolant through the coolant passages machined in the compression plates. A constant temperature water bath (0.5 kW cooling capacity) was used to maintain the temperature of the coolant. Eight heaters (0.8 kW each) placed in line to the coolant flow were used to heat the cell at a rapid rate. A forced heat exchanger cooling unit in-line to the coolant loop provided an additional 2 kW of cooling capacity to increase the rate of cool-down achievable with the system.

2.3. Sensors and measurement

The test stand recorded the test data including the applied load, cell voltage, dew point temperatures and the inlet gas temperatures at a rate of 1 Hz. The errors associated with measuring the load and the cell voltage were 0.25% and 0.5% of the full range respectively. Ten thermocouples, five on each cathode and anode sides, were used to monitor the cell temperature along the length of the channels. The thermocouples were placed in the compression plate and were used to monitor the uniformity of the cell temperatures as shown in Fig. 2. K-type thermocouples were used for their good linear response, with a sheath diameter of 3.175 mm to reduce the influence of adjacent electrical disturbances. The thermocouples have a sheath length of 15.24 cm (6 inches). The materials used for the thermocouple wires are nickel and chromium. Eight additional thermocouples were used to monitor and control the coolant temperatures along with four thermocouples used to monitor and control the gas line temperatures. All thermocouples were calibrated to provide a measurement accuracy of ±1 °C. Two-phase pressure drop across the channels was measured using a differential pressure sensor from Honeywell®, with a range of 35 kPa and an accuracy of 0.25% full scale over the entire range. The resulting uncertainty was less than 0.09 kPa for the readings. A National Instruments (NI) PXIE chassis was used with a custom in-house developed VI to record data.

3. Test procedure

On first assembly, the fuel cell was conditioned at 40 °C by increasing load in intervals of 2.5 A until the cell voltage reached 0.6 V. The load current was updated every 15 min to maintain the cell voltage at 0.6 V for 8 h. At the start of each testing, the cell was operated at 0.6 V for at least 30 min. This allowed the membrane to become sufficiently hydrated and the cell to reach a steady state condition before commencing the test [53]. The flow rates were

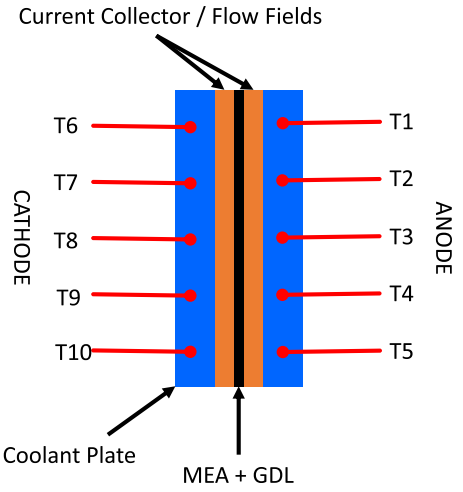

Fig. 2. Location of thermocouples in the compression plate on both anode and cathode sides of the fuel cell.

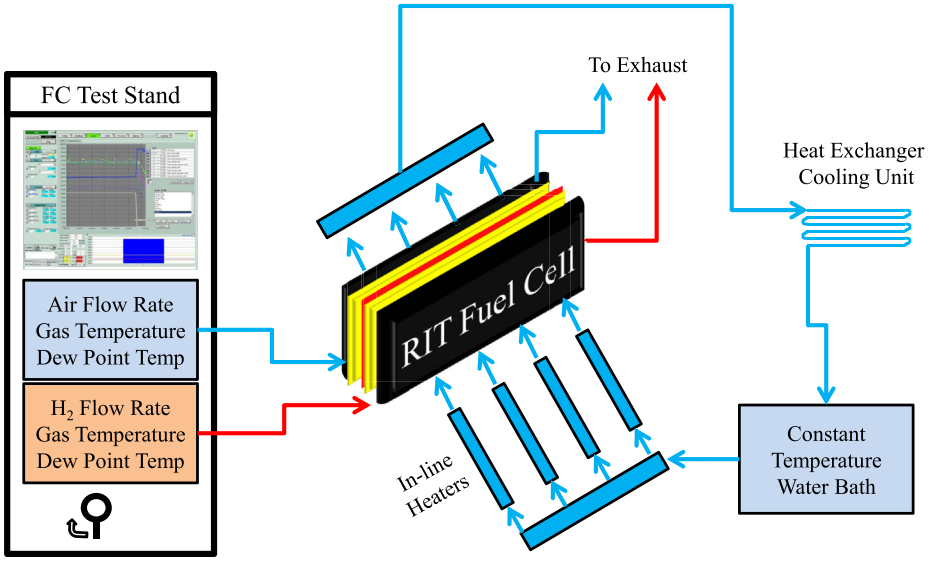

Fig. 1. Schematic of the fuel cell test setup with a Greenlight G40 Test stand to control the fuel cell operating conditions and a constant temperature water bath to control the cell temperature. (For interpretation of the references to color in this figure legend, the reader is referred to the web version of this article.)

controlled by the test stand, maintaining the flow stoichiometry at 2 for cathode and 1.5 for anode throughout the testing.

For steady state testing, the cell was set to the desired conditions and allowed to stabilize for 60 min. This was followed by recording data over 60 min, allowing us to average any fluctuations observed due to the two-phase flow in the flow channels. Pressure drop, cell temperature, cell voltage and the load current were monitored over the entire duration.

For transient testing, the cell was allowed to first reach steady state using the cell conditioning, as described above. For transient load conditions, the cell was maintained at a set temperature to isolate the effects of transient load and transient temperature. The load was increased or decreased by 20 A (0.4 A cm^{-2}) over set time periods of 30 s and 300 s. To obtain a linear ramp during current changes, HyAl FCATS was used. The in-line heaters for the coolant were utilized in implementing rapid increases in temperature for transient temperature study. To decrease the temperature quickly, the heat exchanger cooling unit was used.

For testing the effect of transient temperature changes, the cell temperatures, gas line temperatures, and the dew point temperature were all preset on the control units at the start of the test. The test was considered completed when the cell temperature reached the set point, usually in 900 s for 40 °C change in temperature. The inlet relative humidity was not controlled independently, as it reached the set point based on the temperature of the inlet gases and dew point temperature, both of which respond to temperature changes at a slower rate than the cell temperature.

4. Testing conditions

Two sets of experiments were conducted as part of this investigation. Steady state performance of the cell was monitored with pressure drop data as part of the initial phase of the work. The transient response from the cell was recorded for load changes and temperatures changes. The transient data was compared to the steady state performance to quantify the transient effect of changing load at different temperature conditions during the operation of the cell. The test conditions are setup to match automotive fuel cell operating conditions as discussed by Owejan [54] and provided on www.pemfcdata.org.

Steady state testing was done at two different current densities for each of the three temperatures. This allowed us to gather six different baseline conditions to compare with the transient conditions. Table 1 provides the conditions for steady state testing. The dew point temperature was adjusted such that the inlet relative humidity remained at 95%.

Table 2 shows the transient tests that were conducted as part of this study. Tests 1–6 show positive and negative load changes at steady temperatures of 40 °C, 60 °C and 80 °C. Tests 7–10 focus on transient temperature changes while the load is held constant at 1.0 A cm^{-2}. The two-phase pressure drop from the transient tests was compared with the pressure drop during the steady state conditions.

Table 1
Steady state testing conditions for Phase I testing.

Test#	Cell temperature (°C)	Load (A)	Inlet RH (%)
1	40	30	95
2	40	50	95
3	60	30	95
4	60	50	95
5	80	30	95
6	80	50	95

Single-phase flow is considered when the cell is not operational, i.e. no load current is applied. This assumes that there is no water generation in the cell due to the absence of reaction. Two-phase flow is considered when the cell is operational. With load being applied, the water generation can be calculated using Faraday's law. This water is being introduced into the reactant channels, in liquid or vapor phase. All the results discussed in this work are for two-phase flow conditions.

5. Results and discussion

This section provides the details of the results obtained from the testing at specified conditions as discussed in Section 4. The time required for the system to return to steady state is considered as an important parameter. Results for transient load changes show the variation of cell voltage and pressure drop as a function of time. The results for transient temperature are shown in terms of voltage response and pressure drop as a function of temperature.

5.1. Temporal dependence of pressure drop in PEMFC reactant channels

Previous work has shown that the time duration for transients in the electrochemical processes are very fast (relatively less than 1 s) [24]. However, the two-phase transport within the GDL occurs over a significantly longer time frame [9]. Fig. 3 shows the cathode pressure drop associated with a change in the load from 0.8 A cm^{-2} (40 A) to 0.1 A cm^{-2} (5 A). The system was allowed to stabilize over 2 h, by the end of which it had reached steady state as observed in region A in Fig. 3a. The load was changed, and the air flow rates followed the change in load based on the stoichiometry of 2 for the cathode side (as seen by the drop in pressure). Region B in Fig. 3a is enlarged in Fig. 3b and shows that the pressure drop requires almost 2500 s (over 40 min) in returning to a new steady state value. This shows that the two-phase flow in the gas channels has a transience period of the order of several minutes to an hour.

5.2. Effect of load changes on pressure drop and voltage response

Fig. 4 shows the effect of increasing load on the pressure drop at three temperatures of 40 °C, 60 °C and 80 °C. The load is increased from a current density of 0.6 A cm^{-2} to 1.0 A cm^{-2} over 300 s. It can be observed from the figure that the pressure drop response at the higher temperature is much steeper. At 40 °C, the pressure drop remains high throughout as there is more liquid water present in the channels. The liquid phase component keeps the pressure drop high in the channels. At 60 °C, the saturation pressure is much higher; therefore little liquid water is left in the channels. Thus the pressure drop is significantly lower in the case of 60 °C compared to that at 40 °C. Table 3 and Fig. 5 shows the water vapor uptake into

Table 2
Transient testing conditions for Phase II testing.

Test#	Cell temperature start (°C)	Cell temperature end (°C)	Load start (A)	Load end (A)
1	40	40	30	50
2	40	40	50	30
3	60	60	30	50
4	60	60	50	30
5	80	80	30	50
6	80	80	50	30
7	40	60	50	50
8	40	80	50	50
9	60	40	50	50
10	80	40	50	50

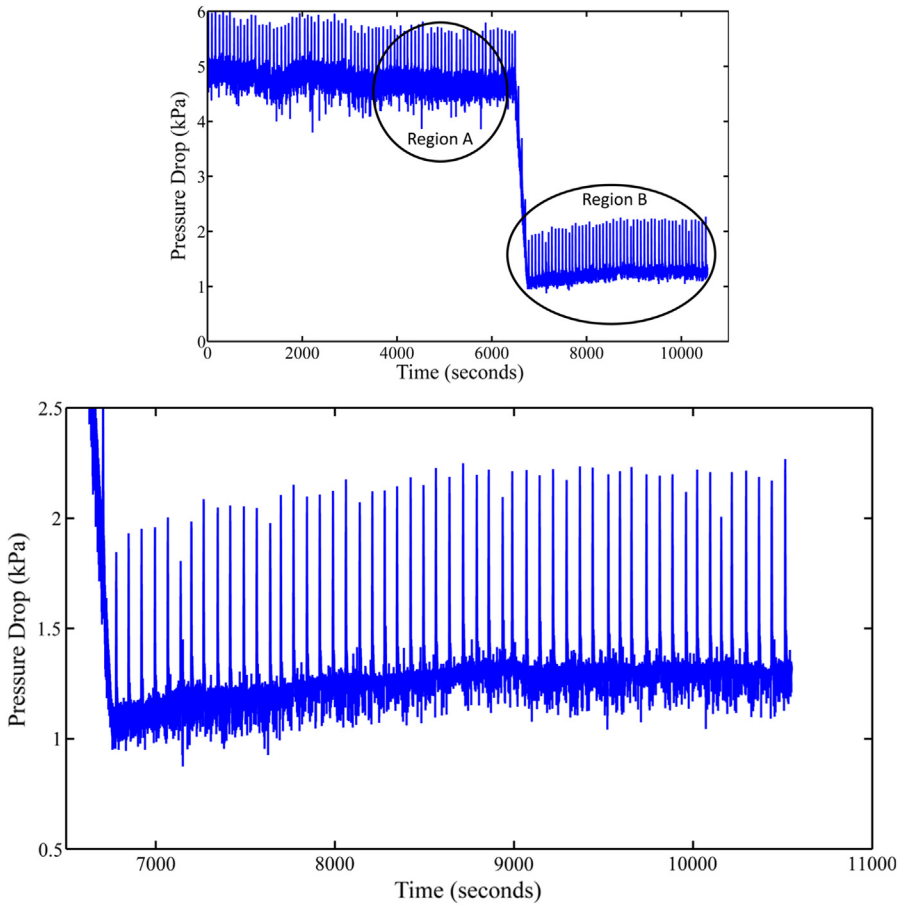

Fig. 3. (a) Time required for the pressure drop to reach steady state after a change in load on the PEMFC. Load changes from 0.8 A cm^{-2} to 0.1 A cm^{-2}. Figure (b) shows the region B, the 4000 s after changing the load.

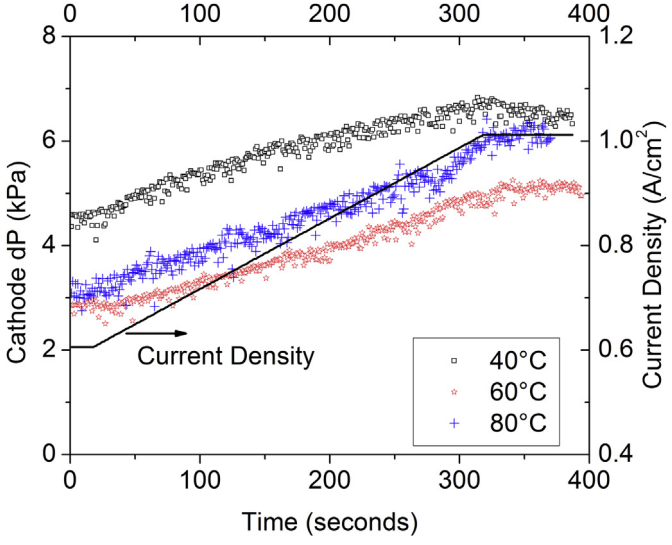

Fig. 4. Effect of increasing load changes on pressure drop for the temperatures of 40 °C, 60 °C and 80 °C as the current density is changed from 0.6 A cm^{-2} to 1.0 A cm^{-2}.

the gas stream at 40 °C, 60 °C and 80 °C with an inlet relative humidity of 95% for each case. At a temperature of 80 °C, over 8% of the water produced can be removed in the vapor stream even with the 95% inlet RH, compared to less than one percent at the lower temperature of 40 °C. At 80 °C, for the lower current density of 0.6 A cm^{-2}, the pressure drop is slightly higher than that at 60 °C because of lower density and greater mass of water vapor being carried in the gas stream. At the higher current density of 1.0 A cm^{-2}, the pressure drop rises more rapidly. It can be observed that the pressure drop response from the change in load is steeper at the higher temperatures. At the lower temperature, there is more liquid water present in the channels as shown in a previous work [44], and therefore the pressure drop is higher. Following the flow pattern study conducted earlier by the authors, at the lower current density, there is a larger contribution of slug flow towards the liquid water in the channels, whereas with increase in the current density, the flow is dominated by film flow [31,32,44].

Fig. 6 shows the effect of decreasing load on pressure drop at the same temperatures. The load is decreased from 1.0 A cm^{-2} to 0.6 A cm^{-2} over a period of 300 s. As seen in Fig. 4, the change in pressure drop is steeper in the case of 80 °C compared to 40 °C. Although the pressure drop at the start of the test (at 1.0 A cm^{-2}) is very similar for both the temperatures, the pressure drop at the end of the test is much higher in the case of 40 °C compared to 80 °C. This again can be attributed to the increased quantity of liquid water at the lower temperatures, compared to that at higher temperatures, where most of the water is in vapor phase due to the higher saturation pressure of water at 80 °C. It is seen that 60 °C is the optimal condition (among the tests conducted) for the fuel cell with the lowest pressure drop, and smooth transition when the load is changed.

Thus, decreasing load at the lower temperatures does not decrease the pressure drop significantly and results in build-up of

Table 3
Water uptake into the gas stream at different temperatures (50 cm^2 of active area matches that of experimental condition).

Current density	Stoich ratio	Water generation	Air flow rate	Inlet RH	Water vapor uptake at operating temperatures		
					40 °C	60 °C	80 °C
A cm^{-2}		mol s^{-1}	mol s^{-1}	%	mol s^{-1}	mol s^{-1}	mol s^{-1}
0.6	2	1.55E-4	3.11E-4	95	6.54E-7	2.31E-6	1.25E-5
0.8	2	2.07E-4	4.15E-4	95	8.73E-7	3.08E-6	1.67E-5
1.0	2	2.59E-4	5.18E-4	95	1.09E-6	3.85E-6	2.08E-5

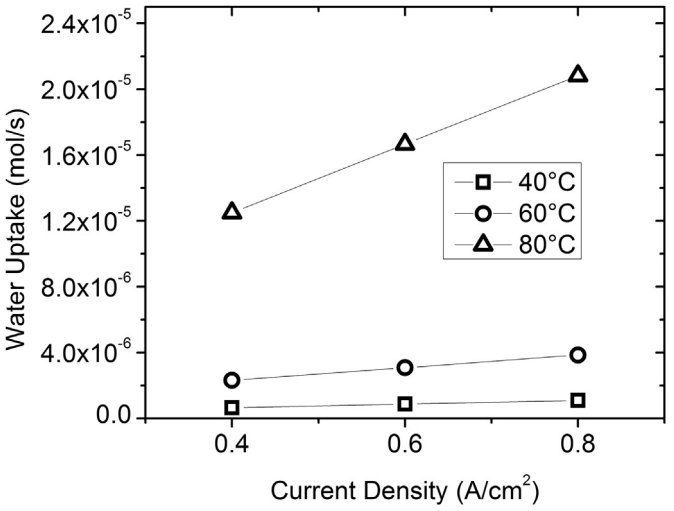

Fig. 5. Water uptake at cell temperatures of 40, 60 and 80 °C with an inlet relative humidity of 95%.

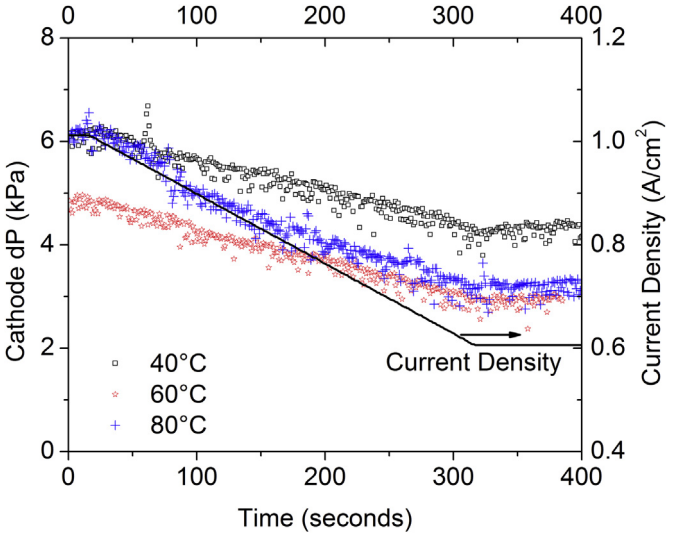

Fig. 6. Effect of decreasing load changes on pressure drop for the temperatures of 40 °C, 60 °C and 80 °C as the current density is changed from 1.0 A cm^{-2} to 0.6 A cm^{-2}.

liquid water within the channels. Therefore, if possible, systems should strive to reduce transient load changes at lower operating temperatures (below 40 °C). However, at higher temperatures, the pressure drop follows rapidly with the reduction in load. Transient load changes at the higher temperatures are not as serious a concern. Fig. 7a shows the spectrum analysis of the pressure drop signal. The power depicts the relative quantity of water being removed as slugs, at the lowest frequency. The frequency vs power diagram for the case of 40 °C with increasing load is shown. The power of the signal for the three different temperatures is compared and shown in Fig. 7b. It can be observed that the power is largest for the temperature of 40 °C and decreases as temperature is increased to 60 °C. As the temperature is further increased to 80 °C, the power increases as seen in Fig. 8b. This could be attributed to the loss in membrane hydration. The water being lost from the membrane gets pushed into the channels resulting in an increase in pressure drop. Additionally, when the load is decreased, the power (in Fig. 7b) is seen to be consistently higher than the cases of increasing load. This reinforces the earlier observations that water hold-up increases when the current density is reduced due to the decrease in the air flow velocity.

5.3. Effect of temperature changes on pressure drop and voltage response

Fig. 8 shows the effect of increasing temperature on the pressure drop and the voltage response of the cell. The load is held constant at 1.0 A cm^{-2}. In Fig. 8a, the temperature was increased from 40 °C to 60 °C. From the illustrations it can be observed that the voltage response improves with increase in temperature from 40 °C to 60 °C. This improvement in voltage response is attributed to the

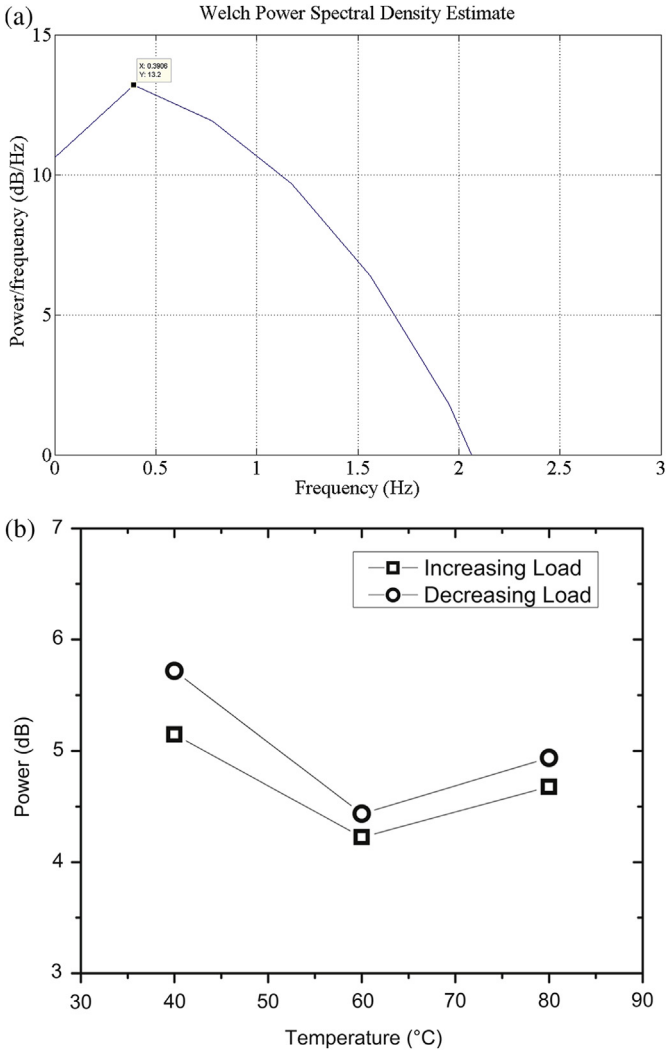

Fig. 7. Spectral analysis of the pressure drop signal. (a) Welch power density plot (b) Power of the water features.

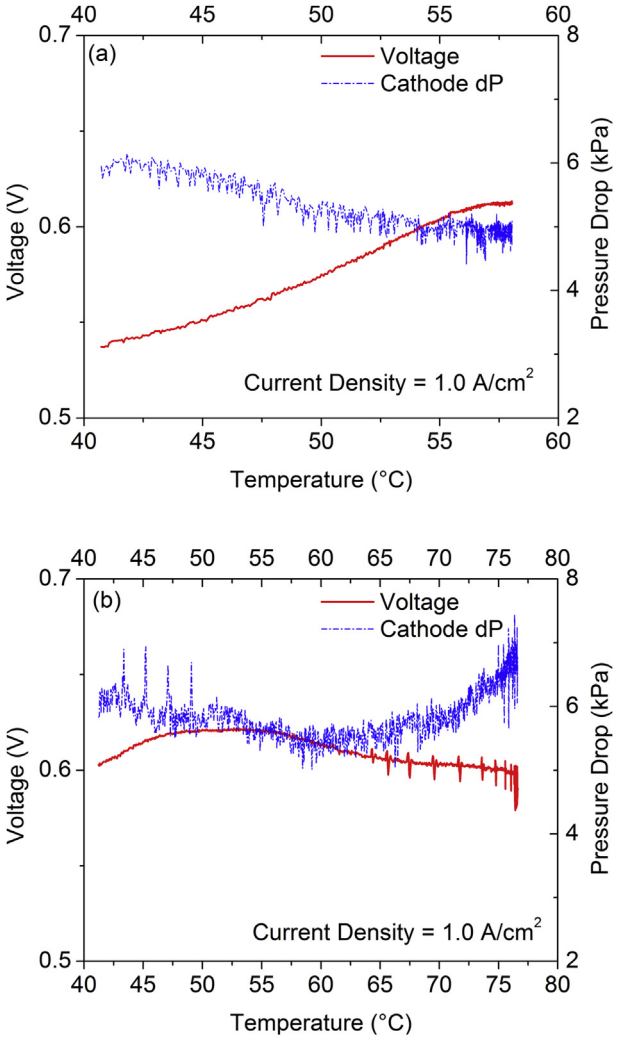

Fig. 8. Effect of increasing temperature on the voltage response and the two-phase pressure drop in the channels, (a) cell temperature increases from 40 °C to 60 °C (b) cell temperature increases from 40 °C to 80 °C.

reduced water flooding in the channels. Reduced water in the reactant channels reduces transport resistance and increases interfacial area available for the transport of reactants to the catalyst layer. The pressure drop decreases with increase in temperature to 60 °C as the saturation pressure increases, and more of the water is transported in vapor phase. This causes the two-phase contribution to decrease and the pressure drop is dictated by the single-phase flow characteristics.

In Fig. 8b, temperature was increased from 40 °C to 80 °C. In the first few seconds, as the temperature increases to 55 °C, the cell voltage increases. Beyond this point, as the temperature continues to rise up towards 80 °C, the voltage begins to decrease. This can be attributed to the rapid increase in temperature, which results in the drying of the membrane. As the cell temperature increases, the GDL begins to dry out followed by the membrane, resulting in a higher proton resistance and therefore a lower cell voltage. The pressure drop begins to increase due to the increase in the single-phase pressure drop as the density decreases with increased temperature. This results in a higher flow velocity. As the investigation is focused on the transient effects, the dew point temperature is changed at the same time as the cell temperature, but the response time of the dew point heater is slow and therefore cannot match the increase in cell temperature. Thus, the relative humidity of the inlet stream also decreases with increasing temperature, further leading to the drying of the membrane.

Fig. 9 shows the effect of decreasing temperature on the pressure drop and the voltage response of the cell at 1.0 A cm^{-2}. In the test represented in Fig. 9a, temperature is decreased from 80 °C to 40 °C in less than 15 min. The cell voltage remains steady until 60 °C, beyond which it drops off. The pressure drop begins to decrease at the start of the test due to the increase in density of the gases resulting in lower gas velocities. However, after the initial dip, the pressure drop remains steady. The decrease in voltage and the steady pressure drop are explained by an increase in liquid water in the channels. The rapidly decreasing temperature increases condensation within the channels, resulting in an increased pressure drop and a higher mass transport resistance. In Fig. 9b, when the temperature is decreased from 75 °C to 55 °C, the drop in temperature is smaller and therefore results in almost no change in cell voltage and a very small decrease in pressure drop. Therefore, reducing temperature rapidly to 55 °C does not result in increased liquid water in the channels. The main concern with decreasing temperature rapidly is seen as temperature falls below 55 °C.

5.4. Comparison of transient and steady state pressure drop

Fig. 10 shows the comparison of transient pressure drop response to the steady state response for temperatures of 40 °C, 60 °C and 80 °C. Two sets of transients observed over 30 s and 300 s are compared with the steady state behavior. Using both transient times, we observe an overshoot when the pressure drop rises or falls following the increase/decrease in the current density and then changes direction until it reaches the steady state condition. The increase in load is matched by an increase in pressure drop, which reaches a peak. The higher peak is associated with the rapid increase in load. This can be attributed to the increased gas flow which encounters the flow resistance due to liquid water already present in the channels. As more of the liquid water is removed by the higher gas velocities, the pressure drop decreases and settles into the steady state value. For the gradual increase in load (over 300 s), the peak is lower and there is less significant transient effect on two-phase flow. This explains the findings of Rabbani and Rokni [19], where the power consumption of the auxiliary systems increased during transient periods.

At the higher temperatures of 60 °C and 80 °C, there is less water in the cathode channels as shown in our prior work [44]. For both rates of changes of load, no distinct peak is observed when the load is changed. The system reaches steady state at a very rapid pace. Consequently, the impact of transients is most significant at the lower temperature operation of PEMFCs. Additionally, it can be seen that the two-phase transient behavior is more prolonged when there is more liquid water in the channels.

6. Conclusions

The effects of transient load and temperature changes on the two-phase flow behavior in the reactant channels of the PEMFC were investigated. An in situ setup was used with an in-house built fuel cell, designed to automotive specifications. Voltage response and the pressure drop in the reactant channels are used to interpret the transient behavior of the PEMFC. The following conclusions can be drawn from the current work.

I. Two-phase flow requires several minutes to return to steady state following a transient event. As automotive powertrains encounter continuously changing power demand; it is therefore a fair assumption that the two-phase flow would never achieve a steady state behavior.

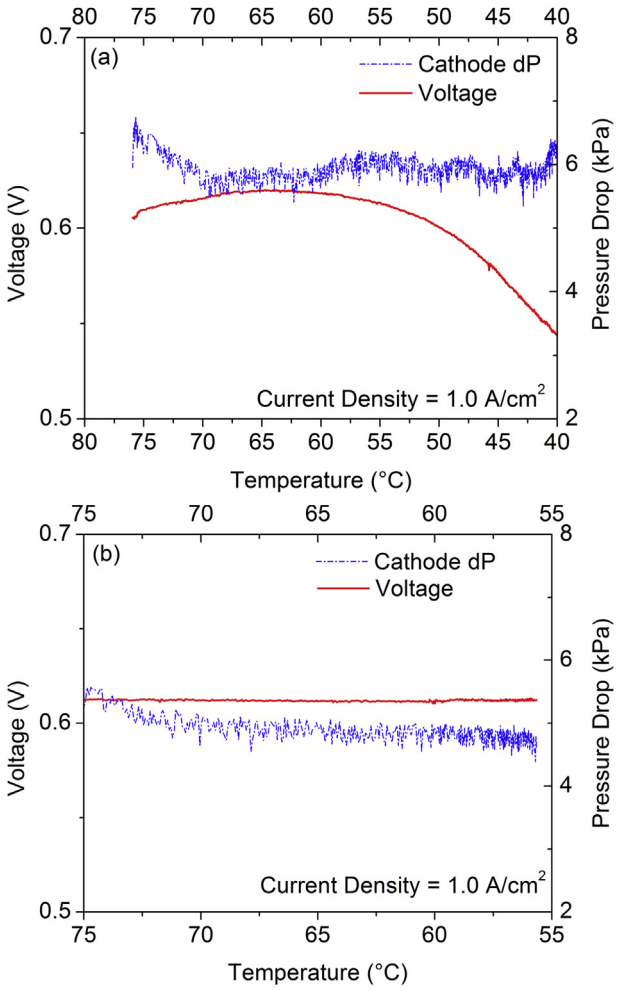

Fig. 9. Effect of decreasing cell temperature on the voltage response and the two-phase pressure drop in the channels, (a) cell temperature decreases from 80 °C to 40 °C (b) cell temperature decreases from 75 °C to 55 °C.

II. Transient load changes are less significant above 60 °C. At the higher temperatures, more water is transported in the vapor form. Therefore, there is less impact of liquid water on the pressure drop in the reactant channels. Transient behavior at the higher temperatures is not as serious a concern.

III. At the lower temperature of 40 °C, decreasing loads result in a longer transient duration compared to increasing loads. This is due to the increased water presence during decreasing loads, as shown by Fig. 7b.

IV. More work needs to be done to remove the water at the lower temperature of 40 °C compared to the water removal at the higher temperatures. Additionally, there is more water to be removed when the load is being decreased compared to increasing load.

V. Two-phase pressure drop reaches steady state more quickly at the higher temperatures. Load changes result in longer transients at the lower temperature of 40 °C, with the pressure drop requiring more than 500 s in returning to a new steady state value. At 60 °C, the two-phase flow reaches steady state within seconds of a load change. At the higher temperature, the transient behavior is less prominent. This can be attributed to increased vapor transport in the channels and therefore less liquid water to introduce two-phase effects.

VI. Overshoot/undershoot is observed in the two-phase pressure drop at 40 °C. Although this phenomenon has been observed in current and voltage response, it had not been

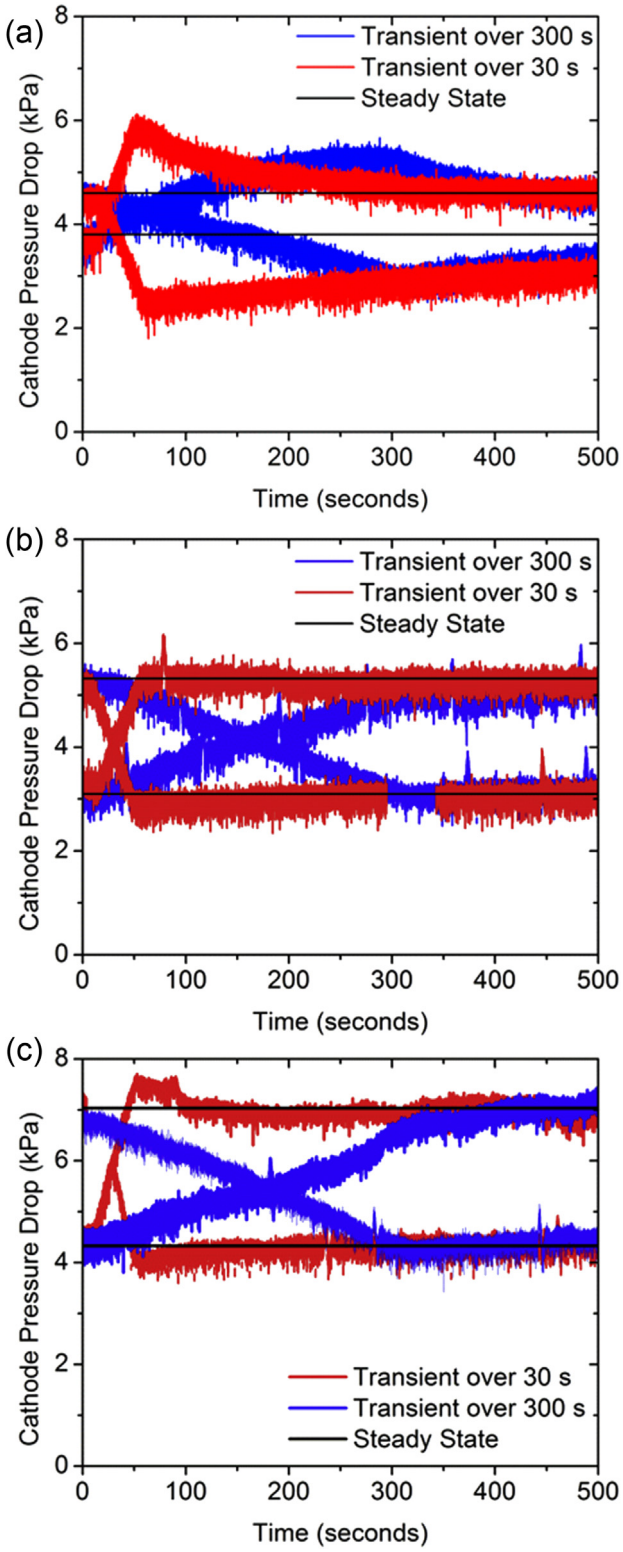

Fig. 10. Comparing steady state and transient response of pressure drop at temperatures of 40 °C, 60 °C and 80 °C for loads of 30 A and 50 A. (Color on web). (For interpretation of the references to color in this figure legend, the reader is referred to the web version of this article.)

reported for two-phase pressure measurements. Tendency for overshoot/undershoot reduces at the higher temperatures of 60 °C and 80 °C.

VII. Increasing temperature to 80 °C leads to membrane dry out and loss in fuel cell performance. With rapidly increasing cell temperature, the performance improves initially (up to 60 °C) due to improved water management and lower liquid water presence in the reactant channels. However, as the cell temperature continues to increase towards 80 °C, the cell performance reduces as the membrane begins to dry out. Therefore, if the cell is being heated beyond 60 °C, it should be slower than done here.

VIII. Decreasing temperature below 60 °C leads to increased condensation and liquid water in the channels. When rapidly cooling the cell, going from 80 °C to 60 °C, the cell performance remains steady. As the temperature continues to decrease below 60 °C, the cell performance starts to decrease. The pressure drop remains high due to increased condensation and larger quantity of liquid water held in the channels. This increases the mass transport resistance and decreases the performance.

Acknowledgments

This work was conducted in the Thermal Analysis, Microfluidics and Fuel Cell Laboratory at the Rochester Institute of Technology. The work was supported by the US Department of Energy under the award number DE-EE0000470. The authors would like to thank Wenbin Gu and Jeffrey Gagliardo from the Electrochemical Energy Research Laboratory at General Motors for supplying the GDL samples tested in this work and for general technical discussions facilitating this work.

References

[1] A.F. Pacheco, M.E.S. Martins, H. Zhao, Fuel 111 (2013) 733.
[2] S.F. Tie, C.W. Tan, Renew. Sustain. Energy Rev. 20 (2013) 82.
[3] P. Corbo, F.E. Corcione, F. Migliardini, O. Veneri, J. Power Sources 145 (2005) 610.
[4] M. Uzunoglu, M.S. Alam, Energy Convers. IEEE Trans. 21 (2006) 767.
[5] J.C. Amphlett, R.F. Mann, B.A. Peppley, P.R. Roberge, A. Rodrigues, J. Power Sources 61 (1996) 183.
[6] J.T. Pukrushpan, H. Peng, A.G. Stefanopoulou, J. Dyn. Syst. Meas. Control 126 (2004) 14.
[7] D. Song, Q. Wang, Z.-S. Liu, C. Huang, J. Power Sources 159 (2006) 928.
[8] W.-M. Yan, H.-S. Chu, J.-Y. Chen, C.-Y. Soong, F. Chen, J. Power Sources 162 (2006) 1147.
[9] Y. Wang, C.-Y. Wang, J. Electrochem. Soc. 154 (2007) B636.
[10] H. Meng, J. Power Sources 171 (2007) 738.
[11] P. Corbo, F. Migliardini, O. Veneri, Int. J. Hydrogen Energy 32 (2007) 4340.
[12] J. Hamelin, K. Agbossou, A. Laperrière, F. Laurencelle, T. Bose, Int. J. Hydrogen Energy 26 (2001) 625.
[13] Y. Tang, W. Yuan, M. Pan, Z. Li, G. Chen, Y. Li, Appl. Energy 87 (2010) 1410.
[14] M.A. Travassos, V.V. Lopes, R.A. Silva, A.Q. Novais, C.M. Rangel, Int. J. Hydrogen Energy 38 (2013) 7684.
[15] S. Kim, S. Shimpalee, J.W. Van Zee, J. Power Sources 135 (2004) 110.
[16] J. Chen, B. Zhou, J. Power Sources 177 (2008) 83.
[17] H. Kim, C.Y. Cho, J.H. Nam, D. Shin, T.-Y. Chung, Int. J. Hydrogen Energy 35 (2010) 3656.
[18] M. De Francesco, E. Arato, J. Power Sources 108 (2002) 41.
[19] R.A. Rabbani, M. Rokni, Sustain. Energy Technol. Assess. 1 (2013) 34.
[20] D. Liu, S. Case, J. Power Sources 162 (2006) 521.
[21] R. Lin, B. Li, Y.P. Hou, J.M. Ma, Int. J. Hydrogen Energy 34 (2009) 2369.
[22] J. Wu, X.Z. Yuan, J.J. Martin, H. Wang, J. Zhang, J. Shen, S. Wu, W. Merida, J. Power Sources 184 (2008) 104.
[23] W. Schmittinger, A. Vahidi, J. Power Sources 180 (2008) 1.
[24] S.-M. Chang, H.-S. Chu, J. Power Sources 161 (2006) 1161.
[25] H. Wu, X. Li, P. Berg, Int. J. Hydrogen Energy 32 (2007) 2022.
[26] F. Chen, Y.-G. Su, C.-Y. Soong, W.-M. Yan, H.-S. Chu, J. Electroanal. Chem. 566 (2004) 85.
[27] J. Stumper, M. Löhr, S. Hamada, J. Power Sources 143 (2005) 150.
[28] J. Wu, X. Zi Yuan, H. Wang, M. Blanco, J.J. Martin, J. Zhang, Int. J. Hydrogen Energy 33 (2008) 1747.
[29] J. Chen, J. Power Sources 195 (2010) 1177.
[30] S.G. Kandlikar, Z. Lu, W.E. Domigan, A.D. White, M.W. Benedict, Int. J. Heat Mass Transf. 52 (2009) 1741.
[31] Z. Lu, S.G. Kandlikar, C. Rath, M. Grimm, W. Domigan, A.D. White, M. Hardbarger, J.P. Owejan, T.A. Trabold, Int. J. Hydrogen Energy 34 (2009) 3445.
[32] Z. Lu, C. Rath, G. Zhang, S.G. Kandlikar, Int. J. Hydrogen Energy 36 (2011) 9864.
[33] M.J. Cheah, I.G. Kevrekidis, J.B. Benziger, Langmuir 29 (2013) 15122.
[34] T. Hellstern, E. Gauthier, M.J. Cheah, J.B. Benziger, Int. J. Hydrogen Energy 38 (2013) 15414.
[35] M.J. Cheah, I.G. Kevrekidis, J.B. Benziger, Langmuir 29 (2013) 9918.
[36] C.D. Rath, S.G. Kandlikar, Colloids Surf. Physicochem. Eng. Aspects 384 (2011) 653.
[37] P. Gopalan, S.G. Kandlikar, J. Electrochem. Soc. 159 (2012) F468.
[38] P. Gopalan, S.G. Kandlikar, J. Electrochem. Soc. 160 (2013) F487.
[39] P. Gopalan, S.G. Kandlikar, Colloids Surf. Physicochem. Eng. Aspects 441 (2014) 262.
[40] M. Grimm, E.J. See, S.G. Kandlikar, Int. J. Hydrogen Energy 37 (2012) 12489.
[41] R. Anderson, L. Zhang, Y. Ding, M. Blanco, X. Bi, D.P. Wilkinson, J. Power Sources 195 (2010) 4531.
[42] K. Tüber, D. Pócza, C. Hebling, J. Power Sources 124 (2003) 403.
[43] J.M. Sergi, S.G. Kandlikar, Int. J. Hydrogen Energy 36 (2011) 12381.
[44] R. Banerjee, S.G. Kandlikar, J. Power Sources 247 (2014) 9.
[45] X.C. Adroher, Y. Wang, J. Power Sources 196 (2011) 9544.
[46] J.E. Steinbrenner, E.S. Lee, C.H. Hidrovo, J.K. Eaton, K.E. Goodson, J. Power Sources 196 (2011) 5012.
[47] L. Zhang, X.T. Bi, D.P. Wilkinson, R. Anderson, J. Stumper, H. Wang, Chem. Eng. Sci. 66 (2011) 3377.
[48] S.G. Kandlikar, Z. Lu, J. Fuel Cell. Sci. Technol. 6 (2009) 044001.
[49] F. Tiss, R. Chouikh, A. Guizani, in:, Elsevier Ltd, 2013, pp. 8532–8541.
[50] W.-M. Yan, F. Chen, H.-Y. Wu, C.-Y. Soong, H.-S. Chu, J. Power Sources 129 (2004) 127.
[51] R. Banerjee, E. See, S.G. Kandlikar, ECS Trans. 58 (2013) 1601.
[52] J.P. Owejan, J.J. Gagliardo, J.M. Sergi, S.G. Kandlikar, T.A. Trabold, Int. J. Hydrogen Energy 34 (2009) 3436.
[53] M. Zhiani, S. Majidi, Int. J. Hydrogen Energy 38 (2013) 9819.
[54] J. Owejan, M. Mench, M. Hickner, S. Kandlikar, T. Trabold, J. Gagliardo, A. Kongkanand, W. Gu, P. Nicotera, DOE Hydrogen and Fuel Cells Program, FY2011 Annual Progress Report (2011) 827. http://www.hydrogen.energy.gov/annual_progress11_fuelcells.html#f.